Future responses of nutrients in the Yellow Sea and East China seas to climate change and riverine inputs

Xinyue Zhang, Jiawei Shen, and Liang Zhao

Key Laboratory of Marine Resource Chemistry and Food Technology, Tianjin University of Science and Technology, Tianjin 300457, China

Abstract. Nutrients are key regulators of marine primary productivity and ecosystem structure in shelf seas. Investigating future changes in nutrients to climate change and riverine inputs is essential for understanding the response of shelf sea ecosystems and for developing effective marine pollution mitigation strategies. In this study, a 3-dimension biophysical-geochemical coupled model was used to study the spatiotemporal distribution of dissolved inorganic nitrogen (DIN) and dissolved inorganic phosphorus (DIP) in the 2010s and the 2050s under the high-emission scenario in the Yellow and East China Seas. Results indicate that in the 2010s, nutrient concentrations generally decrease from inshore to offshore in the surface waters. Seasonally, nutrient concentrations peak in winter. Under the high-emission scenario, the overall spatial distribution of nutrients is largely consistent with the present, with high-DIN changes primarily detected in the Yangtze River estuary–Hangzhou Bay and adjacent waters, while high-DIP changes are mainly found in the western Yellow Sea. Sensitivity experiments further quantify the relative contributions of climate change and human activities to nutrient variations. Results show that elevated riverine inputs mainly affect nearshore waters, whereas climate change exerts a stronger influence on offshore regions.

1 Introduction

The Yellow and East China Seas, as key continental shelf regions in the northwestern Pacific, are among the areas with relatively high marine primary productivity worldwide and play a critical role in regional fisheries and marine ecological security [1–3]. These seas are influenced by multiple dynamic processes, including the Kuroshio Current, freshwater discharge from the Yangtze River, and the East Asian monsoon, resulting in complex water mass structures and nutrient transport patterns [2,4–5]. Nitrogen (N) and phosphorus (P), as the primary limiting nutrients for marine primary productivity, directly regulate phytoplankton community composition and influence regional primary productivity as well as biogeochemical cycles [6–10]. In recent years, under the combined pressures of global climate change and human activities, seawater temperatures in the Yellow and East China Seas have continuously increased, while terrestrial nutrient inputs have risen significantly, leading to intensified coastal eutrophication and frequent ecological disasters such as red tides [11–13], which pose serious threats to regional marine ecosystem stability. Therefore, systematically investigating the variability and driving mechanisms of nutrients under multiple environmental pressures is essential for understanding continental shelf ecosystem processes and developing effective marine environmental management strategies.

Global climate change significantly affects the transport and redistribution of marine nutrients by altering sea surface temperature, ocean circulation, and stratification [14]. For instance, Arheimer et al. [15] used six global climate models coupled with a hydrodynamic model to assess nutrient changes in Swiss river basins under three climate scenarios, finding that by the 2050s, water temperatures would increase significantly and nitrogen concentrations in rivers would rise by 13%, while total phosphorus and total nitrogen in Lake Spirit would increase by approximately 50% and 20%, respectively. Similar trends have been reported by Park et al. [16] and Fang et al. [17]. In marine systems, climate change further modifies nutrient distributions by altering large-scale air–sea interactions. From 1960 to 2022, climate-driven weakening of the East Asian monsoon and enhanced Kuroshio intrusion have directly impacted regional ocean circulation, water column stratification, and the spatial distribution of nutrients such as nitrogen and phosphorus [4,18–20].

Human activities also play a crucial role in driving nearshore nutrient dynamics [21]. Agricultural runoff, urban wastewater, and industrial development have significantly increased nutrient fluxes delivered by rivers to the ocean, altering the spatiotemporal distribution of coastal nutrients [21]. Studies indicate that global riverine nitrogen and phosphorus fluxes increased by 90% and 75%, respectively, over the 20th century [22-23]. Furthermore, projections under the Global Orchestration (GO) scenario suggest that, if current emission trends persist, riverine outputs of dissolved inorganic nitrogen (DIN) and dissolved inorganic phosphorus (DIP) from

Chinese coastal rivers could increase by at least 50% by the 2050s compared to the early 21st century [24], with major rivers such as the Yangtze acting as primary drivers of coastal eutrophication [12, 25]. Although previous studies have characterized the historical spatiotemporal distribution and variation of nutrients in the Yellow and East China Seas [26–30], the response mechanisms of future nutrient changes under the combined influence of climate change and human activities remain poorly understood.

This study uses a three-dimensional physical–ecological coupled model [31] under the CMIP6 SSP5–8.5 scenario to run three experiments: a 2010s baseline, a 2050s combined forcing scenario, and a climate-only scenario with fixed riverine inputs. Comparing these simulations quantifies spatiotemporal changes in N and P and separates the relative contributions of climate change and human activities, offering guidance for marine management and adaptation.

2 Methods

This study uses a three-dimensional physical–ecological coupled model, combining a Princeton Ocean Model (POM) hydrodynamic module with a Norwegian Ecological Model System ecological module. The model domain covers the Bohai Sea, Yellow Sea, and East China Sea (117.5–131.5°E, 24–41°N; Figure 1). A horizontal resolution of 1/18° is adopted to resolve fine-scale coastal hydrodynamics and biogeochemical variability, and the vertical structure is represented by 21 σ layers to adequately capture stratification. The ecological module represents lower trophic level processes, including three dissolved inorganic nutrients (DIN, DIP, and DSi) [31-32]. Water temperature, currents and diffusivity coefficients from the hydrodynamic module was used as inputs to the biological module.

The performance of this model has been previously evaluated and validated in studies by multiple scholars [31–34], showing that the coupled framework reproduces spatial and seasonal patterns of SST, salinity, circulation (e.g., Kuroshio), and nutrients (DIN, DIP). Specifically, Zhao et al. [31] validated the accuracy of the model-simulated seasonal variations of the circulation pattern in the Yellow and East China Seas. Wu et al. [34] verified the model-simulated nitrogen-to-phosphorus (N/P) ratio in the Yellow Sea, and Shen et al. [32] validated the distribution characteristics of nutrient and chlorophyll a (Chl a) concentrations reproduced by the model.

Two simulations were conducted following Shen et al. [32]: R2010, representing 2010s conditions (ERA5 forcing and observed riverine nutrients), and R2050–8.5, representing 2050s under SSP5–8.5 with projected atmospheric forcing, SST, circulation, and a 60% increase in Changjiang DIN/DIP.

Experimental setups are detailed in Shen et al. [32] (Table 1). R2010 represents 2010s climate conditions, while R2050–8.5 simulates the 2050s under CMIP6 SSP5–8.5 forcing (IPCC AR6, 2021), characterized by rapid fossil fuel growth, uneven socio-economic development, and continued population increase, reaching 8.5 W·m^{-2} radiative forcing by 2100.

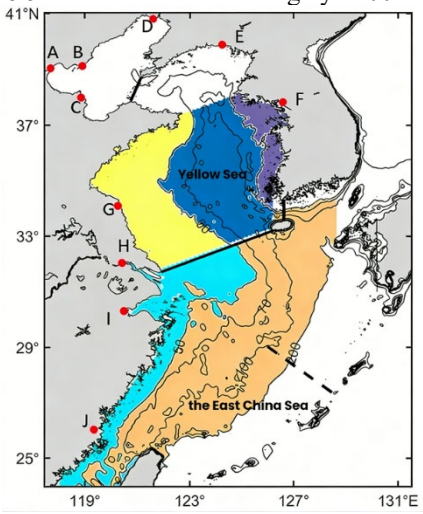

Figure 1. Model domain and subregions. Black lines mark Yellow Sea exchange sections; red dots show ten major river estuaries. Colored areas indicate subregions: western SYS (yellow), central SYS (dark blue), ECS inner shelf (light blue), and ECS mid–outer shelf (orange). Rivers A–J: Haihe, Lehe, Yellow, Liaohe, Dalian, Han, Huaihe, Yangtze, Qiantang, Minjiang.

Table 1. Model configuration.

Experiment	Atmospheric Forcing	Boundary Conditions	Yangtze River Input
R2010	ERA5 (1/4°, 2010 – 2019)	Wang et al., 2019[32]	DIN=77 μmol·L^{-1} DIP=1.0 μmol·L^{-1} DSi=90 μmol·L^{-1}
R2050-8.5	+CMIP6 SSP 5-8.5 (1/2°, 2050 – 2059)	+CMIP6 SSP 5-8.5 (1/4°, 2050 – 2059)	DIN: +60%
R2050-8.5(nGO)	Same as R2050-8.5	Same as R2050-8.5	Same as R2010

To isolate climate-driven effects, a sensitivity experiment, R2050–8.5 (nGO), was conducted with riverine nutrient inputs fixed at 2010s levels while hydrodynamics followed R2050–8.5. Comparing the two scenarios quantifies the contribution of riverine inputs. Nutrient variations across subregions were then analyzed, and relative changes (RC) calculated as follows:

$$RC = \frac{C_{R2} - C_{R1}}{C_{R1}} \times 100\%$$

Here, C represents the nutrient concentration in units of μmol·L^{-1}, and $R1$ and $R2$ denote the two experiments being compared.

3 Results and discussion

3.1 Model validation

Model performance was evaluated by comparing simulated surface DIN and DIP with seasonal

observations (Fig. 2). The model captures key spatial patterns: DIN is highest near the northern Jiangsu coast and Yangtze River estuary and lowest over the East China Sea mid–outer shelf due to Kuroshio influence, with a winter-high, summer-low seasonal cycle. DIP shows similar coastal enhancement and seasonal variability. Overall, the model reliably reproduces both spatial and seasonal nutrient dynamics in the region.

We calculated the cost function (Cost Function, CF), an internationally recognized method for evaluating model performance, and quantitatively verified the simulation results of the spatial distribution and seasonal dynamics of key nutrients in the Yellow Sea. The formula for calculating the cost function is:

$$CF = \frac{\sum|C_s - C_M|}{n \times \sigma_M}$$

the C_s represents the model simulation result, C_M represents the field observation data, n represents the amount of observation data, and σ_M represents the standard deviation of the observation data. This indicator normalizes the average absolute error of the simulation with the standard deviation of the observation data, and can objectively reflect the matching degree between the model simulation values and the measured values. If CF < 1, it indicates excellent model performance; if 1 ≤ CF ≤ 2, it indicates good performance [32–33]. In the Yellow Sea, CF values were 0.20 for SST and 0.74 and 0.71 for DIN and DIP, respectively, all within the "excellent" range. These results demonstrate that the model reliably reproduces the spatial distribution and seasonal dynamics of physical and biogeochemical fields.

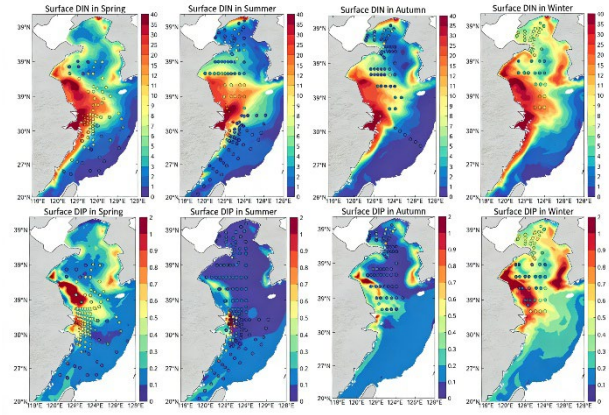

Figure 2. Comparison of modeled (color shading) and observed (circles) surface concentrations of dissolved inorganic nitrogen (DIN, top) and phosphorus (DIP, bottom) in the Yellow and East China Seas across seasons (spring–winter, left to right). Units: μmol·L⁻¹.

3.2 Future changes in Nutrient

3.2.1 Surface DIN

Four representative months (Feb, May, Aug, Nov) were analyzed to capture seasonal variability (Fig. 3). In the 2010s, surface DIN showed a strong nearshore–offshore gradient, peaking at ~35 μmol·L⁻¹ in the Yangtze estuary–Hangzhou Bay due to riverine inputs, while mid–outer East China Sea waters remained low (~6 μmol·L⁻¹) under Kuroshio influence [12,22,25,26]. DIN was highest in winter from monsoon-driven mixing and lowest in summer due to phytoplankton uptake, with spring blooms and autumn declines reflected in monthly changes. Under the SSP5–8.5 2050s scenario, the spatial pattern remained similar, but DIN increased ~30% along the northern Jiangsu coast and Yangtze estuary, with high-change regions extending eastward in summer and southward in winter. Changes were strongest in nearshore areas and the central South Yellow Sea, prompting division into four subregions: western and central South Yellow Sea, and inner and mid–outer East China Sea shelves (Fig. 1).

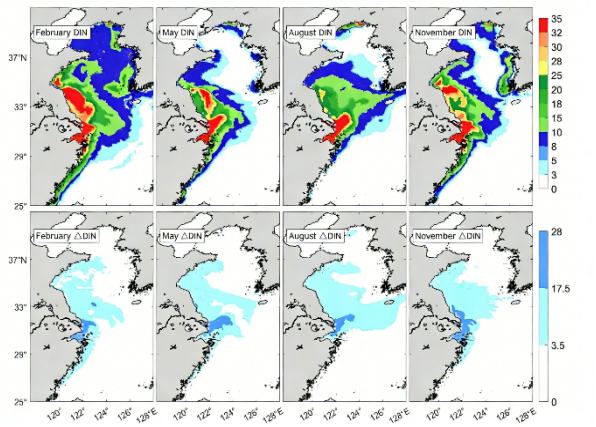

Figure 3. Surface DIN concentrations in the 2010s (panels a–d) and the projected changes in surface DIN under the near-future SSP5-8.5 scenario (panels e–h). Units: μmol·L⁻¹

The relative change (RC) quantifies nutrient responses (Table 2). Surface DIN increases are largest in the East China Sea: inner shelf in spring (38.82%) and winter (39.52%), outer shelf in summer (57.14%), and central South Yellow Sea in autumn (52.18%). High-DIN and high-change zones are mainly on the inner shelves, with moderate-change areas extending west-to-central in winter and eastward toward waters off Jeju Island in summer. showing a strong negative correlation with seasonal phytoplankton biomass [27].

Table 2. Seasonal relative changes of surface nutrients under SSP5-8.5 scenario (RC, %). Note: <5 means no significant change; data are the relative changes in the 2050s compared with the 2010s.

	DIN-Spring	DIN-Summer	DIN-Autumn	DIN-Winter	DIP-Spring	DIP-Summer	DIP-Autumn	DIP-Winter
Western South Yellow Sea	37.86	48.87	47.69	35.02	<5	33.33	20	11.54
Central South Yellow Sea	23.52	44.58	52.18	17.76	23.08	<5	<5	<5

East China Sea Inner Shelf	8.57	5.46	5.27	5.22	<5	<5	<5	15.56
East China Sea Mid-outer Shelf	<5	57.14	<5	<5	13.33	<5	<5	<5

3.2.2 Surface DIP

Surface DIP in the 2010s (Fig. 4a–d) shows coastal enhancement from riverine inputs, especially the Huai and Yangtze Rivers. Concentrations exceed 0.2 μmol·L⁻¹ from Haizhou Bay to Hangzhou Bay, peaking in winter (~2 μmol·L⁻¹) near the Huai estuary, while the Yangtze estuary remains >0.4 μmol·L⁻¹ and the Zhejiang–Fujian coast stays <0.4 μmol·L⁻¹. Under the high-emission scenario, DIP changes vary seasonally: high-change regions (10–50%) occur near northern Jiangsu in spring, expand eastward in summer, shift to Haizhou–Hangzhou Bay in autumn, and concentrate near the Yangtze estuary–Hangzhou Bay in winter (Fig. 4e–h). Seasonal statistics (Table 2) show the largest relative increases in the central South Yellow Sea in spring (23.08%), western South Yellow Sea in summer (33.33%) and autumn (20.00%), and the East China Sea inner shelf in winter (15.56%).

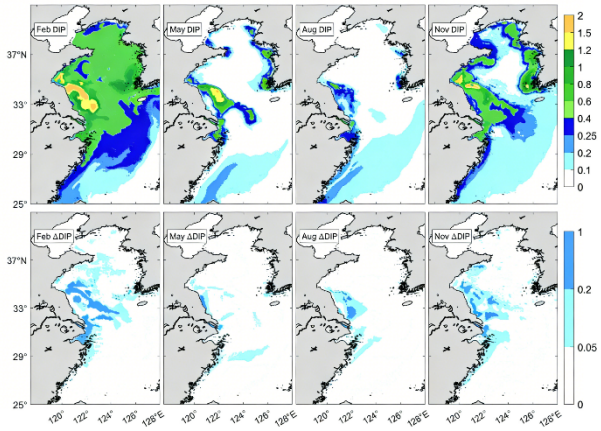

Figure 4. Surface-layer DIP concentrations under the current climate state (2010s, panels a–d) and projected changes under the near-future high-emission scenario (2050s, SSP5-8.5, panels e–h). Units: μmol·L⁻¹.

3.3 Analysis of driving factors

Results indicate substantial nutrient changes in the Yellow and East Seas under the 2050s climate. To quantify the relative contributions of key stressors—climate change and human activities [35]—sensitivity experiments were conducted, comparing climate-only and altered riverine input scenarios to isolate their individual effects on nutrient distributions.

3.3.1 DIN and DIP response to climate change

Table 3 quantifies climate-driven changes in surface nutrients. For DIN, the East China Sea mid–outer shelf is most sensitive, with seasonal relative increases of 21.50% in spring, 15.31% in summer, 12.23% in autumn, and 9.16% in winter. For DIP, responses vary by subregion and season: the central South Yellow Sea shows the largest increases in spring (23.08%) and winter (6.02%), the East China Sea inner shelf peaks in summer (6.25%), and the mid–outer shelf shows the highest change in autumn (8.93%). Overall, climate impacts are strongest in waters deeper than 50 m, particularly over the East China Sea mid–outer shelf.

Table 3. Maximum contribution of driving factors to nutrient changes (RC, %).

Driving Factor	Core Affected Subregion	DIN Maximum Change	Corresponding Season	DIP Maximum Change	Corresponding Season
Climate Change	East China Sea Mid-outer Shelf	21.5	Spring	23.08	Spring
Climate Change	Central South Yellow Sea	12.23	Autumn	6.02	Winter
Riverine Input	Western South Yellow Sea	35.79	Summer	25	Summer
Riverine Input	East China Sea Inner Shelf	31.92	Spring	16	Winter

3.3.2 DIN changes induced by riverine input

Rivers supply land-derived nutrients and strongly influence marine nutrient dynamics [22]. Comparing R2050–8.5 with R2050–8.5(nGO) isolates the effect of riverine inputs. Seasonal relative changes in DIN (Table 3) show the East China Sea inner shelf have the largest increase in spring (31.92%) and winter (30.98%), while the central South Yellow Sea peaks in summer (36.77%) and autumn (38.00%). Overall, riverine inputs primarily affect nearshore regions, with seasonal DIN changes exceeding 30% in SYS-C and the ECS inner shelf.

3.3.3 DIP changes induced by riverine input

Seasonal relative changes (RC, %) of DIP under riverine influence (Table 3) show that the East China Sea inner shelf has the largest increase in spring (14.71%) and winter (16.00%), while the western South Yellow Sea peaks in summer (25.00%) and autumn (14.29%). Overall, riverine inputs mainly impact nearshore areas, with surface waters showing stronger and more extensive changes than deeper layers [36].

4 Conclusions

This study adopted a three-dimensional physical–ecological coupled model combined with the CMIP6 SSP5 high-emission scenario to simulate the

spatiotemporal distributions of dissolved inorganic nitrogen (DIN) and dissolved inorganic phosphorus (DIP) in the Yellow and East Seas under the 2010s (current) and 2050s (near-future) high-emission conditions. Under the 2010s climate state, DIN and DIP concentrations presented a nearshore-high and offshore-low spatial pattern, with higher values in winter and lower values in summer; high concentrations of both nutrients were concentrated in the northern Jiangsu coastal waters (within 50 m depth) and the Yangtze River Estuary–Hangzhou Bay region, while low concentrations were mainly distributed in the middle and outer shelves of the East China Sea. This spatial-temporal pattern is closely related to nearshore anthropogenic inputs (e.g., riverine discharge) and seasonal variations in physical processes such as coastal currents and water mixing, which regulate nutrient transport and diffusion.

Under the 2050s high-emission scenario, the medium- and high-change zones of DIN and DIP were mainly located in the western and central South Yellow Sea and the vicinity of the East China Sea inner shelf, with the most significant changes near the Yangtze River Estuary–Hangzhou Bay; the largest relative change of surface DIN (57.14%) occurred in the middle and outer East China Sea shelf in summer, and that of surface DIP (33.33%) in the western South Yellow Sea. Notably, average DIP concentration changes were relatively moderate due to intensive phytoplankton phosphorus uptake, a key factor mitigating DIP variations. Sensitivity experiments showed that riverine inputs mainly affected nearshore regions, while climate change had more pronounced impacts on offshore areas, with maximum relative changes of 21.50% for DIN and 23.08% for DIP, highlighting their respective regulatory roles. These findings imply that future high-emission climates will alter nutrient distributions in offshore areas, potentially affecting phytoplankton community structure and marine primary productivity, while riverine input management remains crucial for nearshore water quality regulation.

References

1. T. Masubuchi, T. Sakai, M. Yoda, Fish. Sci., **1-18** (2026)
2. J. C. Gong, H. Jin, B. H. Li, Environ. Sci. Technol., **57**, 4039-4049 (2023)
3. C. T. A. Chen, T. H. Huang, C. H. Wu, Sci. Rep., **11**, 5080 (2021)
4. Y. N. Sasaki, C. Umeda, J. Clim., **34**, 4803-4815 (2021)
5. D. Z. Yang, B. S. Yin, Y. J. Hou, Acta Oceanol. Limnol. Sin., **48**, 1196-1202 (2017)
6. Y. J. Tak, Y. K. Cho, J. Hwang, Y. Y. Kim, Front. Mar. Sci., **8,** 785377 (2022)
7. Y. Tian, K. K. Wang, G. P. Yang, Environ. Sci. Technol., **55**, 3668-3675 (2021)
8. Y. Liu, X. Mao, J. Shi, Y. Luo, X. Guo, Y. Wang, Mar. Pollut. Bull., **208**, 116992 (2024)
9. N. Zhou, G. L. Zhang, S. M. Liu, Mar. Pollut. Bull., **176**, 113420 (2022)
10. Y. Gao, H. B. Jiang, J. Mar. Environ. Sci., **40**, 798-804 (2021)
11. P. M. Glibert, Mar. Pollut. Bull., **124**, 591-606 (2017)
12. J. Zhou, X. Liu, E. A. Laws, Geophys. Res. Lett., **53**, e2025GL121124 (2026)
13. K. Chen, K. Li, G. Tan, P. Gao, Water Res., **125278** (2026)
14. S. Sun, A. F. Thompson, J. Yu, et al., Nat. Commun., **15**, 7727 (2024)
15. B. Arheimer, J. Andréasson, S. Fogelberg, AMBIO, **34**, 559-566 (2005)
16. S. Park, G. Kim, H. K. Kwon, Mar. Pollut. Bull., **192**, 115012 (2023)
17. Z. Fang, T. Feng, Y. Meng, et al., J. Geophys. Res. Oceans, **130**, e2024JC021553 (2025)
18. H. J. Tan, R. S. Cai, J. G. Du, Trans. Atmos. Sci., **45**, 489-501 (2022)
19. Y. Dai, S. Yang, D. Zhao, Nature, **615**, 280-284 (2023)
20. R. S. Cai, Z. Q. Han, Z. X. Yang, Adv. Clim. Change Res., **16,** 12 (2020)
21. Q. Lin, Z. Song, M. Qi, Water Res., **125140** (2025)
22. J. A. Ural, C. Kroeze, E. Meers, Mar. Environ. Res., **197**, 106446 (2024)
23. X. Liu, A. H. W. Beusen, L. P. H. Van Beek, Water Res., **142**, 246-255 (2018)
24. H. J. Qu, C. Kroeze, Sci. Total Environ., **408**, 2075-2086 (2010)
25. J. Peng, Z. Wang, C. Cheng, Mar. Pollut. Bull., **223**, 11888 (2026)
26. J. Xiao, X. Chen, L. Zhou, H. Zhang, X. Hang, Y. Chen, Water, **17**, 2469 (2025)
27. J. Wu, Z. Wang, J. Tian, et al., Mar. Environ. Res., **194**, 106338 (2024)
28. L. A. Ye, L. B. Wang, Z. F. Jiang, (2017)
29. Z. Y. Han, C. Qin, W. W. Zheng, J. Ocean Univ. China, **53**, 85-94 (2023)
30. M. A. Kalhoro, V. Chinta, M. Tahir, Algae, **40** (2025)
31. L. Zhao, X. Guo, Ocean Sci., **7**, 27-43 (2011)
32. J. W. Shen, L. Zhao, H. Wei, J. Geophys. Res. Atmos., **128**, e2023JD038737 (2023)
33. J. W. Shen, L. Zhao, H. Wei, Mar. Pollut. Bull., **225**, 119282 (2026)
34. Y. H. Wu, J. Zhang, L. Zhao, et al., J. Tianjin Univ. Sci. Technol., **36**, 30-40 (2021)
35. N. Wang, Y. Li, P. C. Yang, J. Appl. Oceanol., **42**, 178-186 (2023)
36. R. A. Duce, J. LaRoche, K. Altieri, Science, **320**, 893-897 (2008)